Nanoscale

Accepted Manuscript

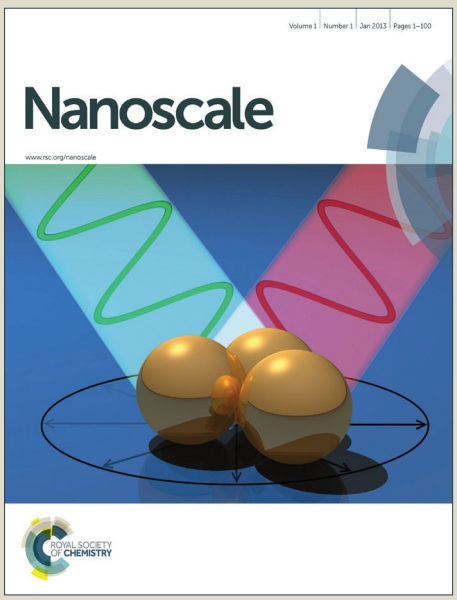

ROYAL SOCIETY OF CHEMISTRY

www.rsc.org/nanoscale

Addressing asymmetry of the charge and strain in a two-dimensional fullerene peapod

V. Valeš[a], T. Verhagen[b], J. Vejpravová[b], O. Frank[a] and M. Kalbáč[*a]

[a]J. Heyrovský Institute of Physical Chemistry, CAS, v.v.i., Dolejškova 3, 182 23 Praha, Czech Republic

[b]Institute of Physics, CAS, v.v.i., Na Slovance 2, 182 21 Praha, Czech Republic

We prepared two-dimensional C_{70} fullerene peapod by a sequential assembly of ^{12}C graphene, C_{70} fullerenes and ^{13}C graphene. The local changes in the strain and doping were correlated with the local roughness revealing an asymmetry in the strain and doping with respect to the top and bottom graphene layers of the peapod.

Introduction

Fullerene peapods represent a new type of bottom-up engineered material consisting of fullerenes and single-walled carbon nanotubes (SWCNTs). The C_{60} fullerene peapods were first observed by Smith in 1998.[1] Since their discovery, fullerene peapods have attracted substantial attention and peapods containing different fullerenes were prepared and characterised.[2–4] As compared with SWCNTs, new effects can be observed in peapods, such as an abnormal temperature dependence of Coulomb blockade oscillations.[5] Fullerene peapods thus extend the range of potential applications of carbon nanostructures in data storage,[6] nanoelectronics[7] or quantum computing.[8] In addition, the properties of fullerene peapods can be further tuned by electrochemical charging[9,10] or by chemical doping.[11]

Fullerene peapods are considered as one-dimensional (1-D) materials because their dimensionality is defined by the SWCNTs. Nevertheless, it should be possible to prepare analogous material in two dimensions as well by encapsulating fullerenes between two layers of graphene. In the two-dimensional (2-D) system, the tunability of the peapod can be further extended and also new areas of application can be opened. However, in contrast to 1-D

peapods, the 2-D materials are more sensitive to the environment. In particular, the substrate significantly influences the properties of the 2-D nanostructures. In the case of 2-D peapods, the substrate is expected to interact only with one site of the 2-D peapod and thus it will create an asymmetry in the strain and doping. This asymmetry can be beneficial as it can provide another degree of freedom for the tunability of such new materials; however, it is necessary to be able to control and quantify such an asymmetry.

The interactions between graphene and other nanosized objects are important, as was demonstrated recently for nanoparticles[12,13] and fullerenes[14,15] on graphene. In particular, fullerenes can act as p-dopants for graphene[15–18] because they are good electron acceptors. Consequently, heterostructures consisting of graphene and fullerenes can exhibit new properties due to the interfacial electronic interactions and charge transfer.[14] On the other hand, the presence of fullerenes might cause delamination of graphene from the substrate, which locally reduces the interaction between graphene and the Si/SiO_2 substrate.[19,20] Furthermore, fullerenes may also affect the strain in the graphene layer, which can further modulate the electronic properties of graphene.[21–23] Experimental studies on the interactions between fullerenes and graphene have been limited to C_{60} up until now. Nevertheless, it has been predicted theoretically that C_{70} interacts with graphene more strongly than C_{60}.[24]

In this work, we prepared new 2-D peapods consisting of C_{70} fullerenes sandwiched between two isotopically labelled graphene layers. Using atomic force microscopy (AFM) and Raman spectroscopy we studied the doping and strain in the top and bottom graphene layers. Because of carbon isotope labelling of graphene layers,[25–27] the characteristic Raman bands can be easily distinguished for bottom ^{12}C and top ^{13}C graphene layers. This enabled us to follow independently the Raman features of the bottom and top layers of the 2-D peapod. Furthermore, we measured and analysed the atomic force microscopy (AFM) and Raman maps in the same area, which enabled us to relate directly the surface topography to strain and doping obtained from the Raman measurements.

Results and discussion

The different Raman shifts of the bands of the bottom (^{12}C) and the top (^{13}C) graphene layers result from the different atomic masses of the isotopes used. The relation between the Raman shift of the ^{13}C graphene (w_{13}) compared with the ^{12}C graphene (w_{12}) reads:

$$w_{13} = w_{12}\sqrt{\frac{12+c_0}{13+c_{13}}},$$

where c_0 is the portion of ^{13}C in the natural methane gas (c_0 = 0.0107) and c_{13} is the concentration of ^{13}C in the enriched gas (c_{13} = 0.99).[25]

A typical Raman spectrum of the graphene ^{12}C/C_{70}/graphene ^{13}C 2-D peapod is shown in Fig. 1. The D, G and 2D bands are the most prominent Raman modes in graphene. The D mode is associated with the presence of defects, the G mode originates from the doubly degenerate phonon mode in the centre of the Brillouin zone, and the 2D mode originates from a second-order process involving two transversal optical (iTO) phonons.[28] All of the peaks were fitted using a pseudo-Voigt line shape. Both of the G bands (for the ^{12}C and the ^{13}C isotopes) exhibited a clear asymmetry that could be fitted only with an additional peak located at a lower wavenumber. The main higher frequency G peak is denoted as G_1, while the additional peak is denoted as G_2. The appearance of the G_2 peak is typically associated with the presence of wrinkles on graphene, as was demonstrated recently.[20] The 2D Raman band of graphene shows an asymmetry as well, however, this asymmetry can be fully fitted with a single pseudo-Voigt line shape. Thus, the obtained peak parameters are the peak area (A), the Raman shift (w), full width at half maximum (FWHM) and the pseudo-Voigt parameter that describes the Lorentzian fraction of the peak. Apart from the described modes, the D′ and the G* modes were fitted as well, as they overlap with the G and 2D bands, respectively. Note that the different intensity of the ^{12}C 2D band compared with the ^{13}C 2D band is caused presumably by a different level of doping of the bottom and top graphene layers, as we discuss later. The AFM images addressing the spatial distribution of fullerenes at the bottom graphene layer are shown in Figure S1 (see Supporting Information for details).

The ^{12}C graphene/C_{70}/^{13}C graphene peapod was measured in exactly the same sample area both by Raman spectroscopy and AFM to describe directly the influence of the surface topography on the Raman spectra. The obtained results are shown in Fig. 2. In the AFM topography image (Fig. 2(a)), local delamination of the ^{13}C top graphene layer from the ^{12}C graphene because of the presence of fullerenes can be observed. However, to be able directly to compare the data obtained from Raman spectroscopy measurements and AFM imaging, the AFM data have to be scaled on the grid defined by the spatial resolution of the Raman spectroscopy measurements (Fig. 2). Raman spectroscopy is sensitive to strain and doping of graphene and we assume that wrinkling of graphene induced by the presence of fullerenes will affect these properties. However, the spatial resolution of Raman spectroscopy is given by the size of the laser spot, which is about 500 nm in diameter. Therefore we transformed the AFM maps by calculating local roughness in terms of local root-mean-square deviations, in the area corresponding to the size of the laser beam (a circle with a diameter of 500 nm) in the points where the Raman maps were measured. In this way, we can attribute the local roughness in a particular spot to the particular Raman spectrum at each point of the Raman map (Fig. 2(b)).

A correlation analysis of the G and the 2D Raman bands of graphene[29] was employed to quantify strain and doping in the top and bottom graphene layers of the 2-D peapod for each point of the Raman map. For the analysis, we assume only a biaxial strain. In the phase space of the position of the G and 2D bands, p-doping causes a shift along a line with a slope of 0.7, while biaxial strain causes a shift along a line with a slope of 2.45. It has been shown that the strain sensitivity of the G position is –57 cm^{-1}/1% of strain[30] and it is linear both for small tensile and compressive strains.[31] The quantification of the doping level is more complicated and was calculated according to theoretical predictions employing time-dependent perturbation theory.[32] The calculation of both strain and doping was performed using the G_1 peak.

First, we calculated the median values of doping and strain from the measured Raman maps. The average doping of the top ^{13}C graphene layer was estimated to be $(2.3 \pm 0.3) \times 10^{12}$ cm^{-2} while the average doping of the bottom ^{12}C graphene layer was estimated to be $(4.5 \pm 0.8) \times 10^{12}$ cm^{-2}. These results show that the top layer is efficiently isolated from the substrate by the bottom graphene layer and the fullerenes. The average strain of the top ^{13}C graphene layer was found to be (-0.126 ± 0.006)% while the average strain of the bottom ^{12}C graphene layer was found to be (-0.102 ± 0.008)%. The slight difference in the average strain values for the top and bottom layers is probably caused by local inhomogeneities, as we discuss later.

Now, we focus on the ^{13}C top graphene layer in more detail, employing a correlation analysis of the Raman and AFM data. In the delaminated part of the top layer we expect lower doping due to lower interaction of the top graphene layer with the ^{12}C bottom graphene layer and the Si/SiO_2 substrate. Because the characteristic size of the delaminated graphene area is small compared with the size of the focused laser beam, in one spot we can see a contribution both from graphene lying on the substrate and from the delaminated graphene. In other words, parts of differently doped graphene contribute to the spectrum within a Raman laser spot. Doping strongly affects the position of the G mode.[33] For this reason, one can see one main peak, G_1, coming presumably from the graphene lying on the surface and a smaller peak, G_2, located at lower wavenumber, coming presumably from less doped delaminated parts of graphene.[20]

The area of the G_2 peak compared with the G_1 peak of the ^{13}C top graphene layer peak is plotted in Fig. 2(d). By comparing the map of the G_2 peak area (Fig. 2(d)) with the root-mean-square deviation map (Fig. 2(b)), regions of less rough surface corresponding to the lower G_2 peak area and regions of more rough surface corresponding to the higher G_2 peak area can be clearly observed. For example, around the centre of the maps, an island of higher local roughness and the higher G_2 area can be clearly seen. This confirms our assumption that the more delaminated graphene areas within the laser spot correspond to the higher area of the G_2 peak. This observation is in agreement with the previous results obtained on graphene

deposited over nanoparticles.[20] For comparison we also measured the surface topography of a blank sample -graphene bilayer without fullerenes, (Fig S1 (d)). It can be clearly seen that the surface of the constructed graphene bilayer is relatively flat as compared with the 2-D peapod sample. Although there are few wrinkles on graphene bilayer, their occurrence and height is much smaller than in the case of the 2-D fullerene peapod. Thus we conclude that a vast majority of the wrinkles present in the 2-D fullerene peapod is induced by the presence of fullerenes. In addition the average height and distances between wrinkles on the top graphene layer of 2-D peapod correspond to the size and distribution of fullerenes/ fullerene aggregates.

Note that few wrinkles originating from the transfer procedure can be observed also on the bottom graphene layer as show in Fig S1 (a).

In order to describe the relationship between the surface roughness and the G_2 mode qualitatively, we made a correlation plot of the local roughness obtained from AFM and the relative G_2 peak area obtained from Raman spectroscopy (Fig S3). The raw data points are scattered and no clear dependence can be seen. Therefore, we binned each 100 adjacent points from the correlation plot of the relative G_2 peak area and calculated the median value, which improved the statistics and the dependence became more obvious (Fig. 3 (a)). The first and third quartiles are depicted as well to demonstrate the degree of dispersion of the data points. It can be seen that with increasing surface roughness the relative G_2 peak area of the top layer is indeed increasing. There is an area near the bottom left corner where there are no Raman data. This is caused by the fact that in this region the ^{12}C bottom and the ^{13}C top graphene layers are oriented close to AB stacking, which gives rise to an additional band between ^{12}C 2D and ^{13}C 2D, involving phonons from both layers.[28,34] Because of the presence of this additional band, it was impossible to fit properly the positions of the ^{12}C 2D and ^{13}C 2D bands, which is necessary for the estimation of the strain and doping in both graphene layers.

Fig. 2(c) shows the strain distribution at different points of the ^{13}C top layer calculated from the correlation analysis of the positions of the G_1 and 2D bands. The overall strain of the graphene top layer is compressive over the whole measured area. We again binned each 100

adjacent points in the correlation plot of the strain of the top ^{13}C graphene layer and calculated the median value with corresponding local surface roughness. The correlation of strain in the top graphene layer and the local roughness in the measured maps reveals a clear trend (Fig. 3(b), S4(b)). The analysis of the correlation plot of strain and the local roughness shows that, with increasing local surface roughness, the absolute value of strain is decreasing. In other words, the more fullerenes that are locally present, the more efficiently is the strain in graphene relaxed. Because our correlation analysis takes into account only the G_1 peak, we can conclude that the strain is released in an area large enough that it affects the whole Raman laser spot.

The analysis of the doping at different Raman spots for the ^{13}C top graphene layer of the 2-D peapod, obtained from the correlation analysis of the positions of the G_1 and 2D bands, did not reveal any obvious correlation of the doping with the local roughness, which is also apparent from the correlation plot of doping and roughness (Fig. 3 (c), S4(c)), where no tendency is observed. Thus, we concluded that the weaker doping of the ^{13}C top graphene layer is localized only in the delaminated part, while the graphene lying on the ^{12}C bottom graphene layer is doped from the substrate. Therefore, doping calculated from the main, G_1, peak does not show correlation with the roughness magnitude and thus a weaker doping in the delaminated part of graphene is solely mirrored in the intensity of the G_2 peak, as shown in Fig. 3(a).

The correlation of the local surface roughness and Raman parameters of the ^{12}C bottom graphene layer of the 2-D peapod is obviously not so straightforward. The area of the G_2 peak of the bottom layer of the 2-D peapod is slightly higher overall compared with the top layer, and it is independent of the local surface roughness Fig. 3(d), which is expected because the bottom layer should not be delaminated by fullerenes. A slightly larger intensity of the G_2 band for the ^{12}C bottom graphene layer as compared with the ^{13}C top layer can be caused by fitting artefacts resulting from an overlap of the ^{12}C G_2 mode with the ^{13}C D′ graphene band.

There is a systematic tendency in the correlation of the local surface roughness and both strain and doping of the bottom graphene layer of the 2-D peapod. In particular, the surface roughness is higher in areas where the bottom graphene layer is more doped and less strained, Fig. 3(e,f). Hence, it seems that fullerenes tend to aggregate preferentially on less-strained graphene areas. This is reasonable result, because the relaxed parts presumably correspond to the local minima. We note that in the case of doping of the bottom graphene layer, no competition between delamination of the graphene layer from the substrate and electronic interaction with fullerenes is expected because they are deposited on the bottom layer.

We assume that the wrinkling of the ^{13}C top graphene layer induced by fullerenes can be described by local roughness, expressed as a root-mean-square deviation. The effect of the presence of fullerenes on the graphene layer covering the fullerenes is clear. The more fullerenes that are located in a single laser spot, the higher relative G_2 peak area is observed. This validates the concept of sub-micron doping inhomogeneities within a single laser spot, which assumes that part of the irradiated graphene is more doped (graphene lying on the surface) while the other part (delaminated graphene) is not in contact with the substrate and therefore it is significantly less doped. Our results are also in agreement with the Raman study on graphene covering iron oxide nanoparticles,[20] where a higher concentration of nanoparticles induced a higher relative area of the G_2 peak.

In general, both of the graphene layers of the 2-D peapod are compressed. This strain probably comes from the transfer process onto the Si/SiO_2 substrate and also from the presence of fullerenes. The magnitude of the compression is comparable with the strain in transferred chemical vapour deposition (CVD) graphene (without fullerenes).[35] From the correlation analysis of strain and local surface roughness, it follows that strain in the ^{13}C top graphene layer tends to be smaller with a higher amount of fullerenes. This means that a high concentration of fullerenes can release the strain in the covering graphene layer. This property of fullerenes is expected as they have been used for their lubricant behaviour.[36] No systematic tendency in the correlation of local surface roughness and doping calculated from the

positions of the G_1 and the 2D peaks was observed. Local changes of doping induced by the presence of fullerenes are localized in the delaminated areas of graphene only. In a single laser spot there are several delaminated areas, therefore this effect is fully described by the relative area of the G_2 peak. The fullerenes tend to aggregate on the bottom graphene layers in spots with lower compression. The presence of fullerenes expressed as local roughness increases the p-doping of the bottom graphene layer, as can be expected from the electronic interactions between graphene and C_{70}.

Conclusion

In summary, we prepared a 2-D peapod consisting of C_{70} fullerenes sandwiched between two isotopically labelled graphene layers. We compared directly the Raman and AFM maps measured in the same area by calculating the local roughness from AFM corresponding to the scale of a Raman spot size. This enabled us to describe local effects of the presence of fullerenes on both graphene layers. We concluded that the presence of fullerenes induces delamination of the top graphene layer from the bottom layer, which is demonstrated by a local decrease of doping on a sub-micron scale. We also found that fullerenes enable local release of strain in the top graphene layer.

Experimental

The heterostructure consisted of C_{70} fullerenes sandwiched between two graphene layers. First, the bottom ^{12}C graphene was grown using the CVD process[37,38] on a copper substrate and subsequently transferred onto a clean Si/SiO_2 substrate (pre-treated in oxygen plasma) using poly(methyl methacrylate) (PMMA) according to procedures reported previously.[37] The majority of PMMA was removed by acetone and the PMMA residuals were eliminated by a careful heating at 300 °C. Fullerenes were spin-coated from a hexane solution onto the

substrate with the ^{12}C graphene layer. Finally, the top ^{13}C graphene was grown using CVD with ^{13}C methane as a reaction precursor and transferred using PMMA in the similar way as the bottom layer over the deposited fullerenes.

The AFM images were measured with a Bruker Dimension Icon using Scanasyst-air silicon nitride probes. The measurements were performed in the PeakForce tapping mode with the peak force setpoint of approximately 1 nN and with a resolution of 512 lines. The images were further processed using Gwyddion software.[39]

The Raman spectra were measured using a WITec alpha300 R spectrometer equipped with a piezo stage with 532 nm excitation wavelength. The laser power was kept below 1 mW to avoid any heating effects. The laser was focused on the sample with a 100× objective to a spot with a diameter of around 500 nm.

Acknowledgements

The work was supported by Czech Science foundation contract No.P208121062.

References

1 B. W. Smith, M. Monthioux and D. E. Luzzi, *Nature*, 1998, **396**, 323–324.

2 H. Kataura, Y. Maniwa, M. Abe, A. Fujiwara, T. Kodama, K. Kikuchi, H. Imahori, Y. Misaki, S. Suzuki and Y. Achiba, *Appl. Phys. A Mater. Sci. Process.*, 2002, **74**, 349–354.

3 M. Kalbáč, L. Kavan, M. Zukalová, S. Yang, J. Čech, S. Roth and L. Dunsch, *Chem. - A Eur. J.*, 2007, **13**, 8811–8817.

4 V. Zólyomi, H. Peterlik, J. Bernardi, M. Bokor, I. László, J. Koltai, J. Kürti, M. Knupfer, H. Kuzmany, T. Pichler and F. Simon, *J. Phys. Chem. C*, 2014, **118**, 30260–30268.

5 P. Utko, R. Ferone, I. V Krive, R. I. Shekhter, M. Jonson, M. Monthioux, L. Noé and J. Nygård, *Nat. Commun.*, 2010, **1**, 37.

6 Y.-K. Kwon, D. Tománek and S. Iijima, *Phys. Rev. Lett.*, 1999, **82**, 1470–1473.

7 H. Y. Yu, D. S. Lee, S. H. Lee, S. S. Kim, S. W. Lee, Y. W. Park, U. Dettlaff-Weglikowskaand and S. Roth, *Appl. Phys. Lett.*, 2005, **87**, 163118.

8 S. C. Benjamin, A. Ardavan, G. A. D. Briggs, D. A. Britz, D. Gunlycke, J. Jefferson, M. A. G. Jones, D. F. Leigh, B. W. Lovett, A. N. Khlobystov, S. A. Lyon, J. J. L. Morton, K. Porfyrakis, M. R. Sambrook and A. M. Tyryshkin, *J. Phys. Condens. Matter*, 2006, **18**, S867–S883.

9 L. Kavan, L. Dunsch, H. Kataura, A. Oshiyama, M. Otani and S. Okada, *J. Phys. Chem. B*, 2003, **107**, 7666–7675.

10 J. Tarábek, L. Kavan, M. Kalbáč, P. Rapta, M. Zukalová and L. Dunsch, *Carbon N. Y.*, 2006, **44**, 2147–2154.

11 M. Kalbáč, V. Vales, L. Kavan and L. Dunsch, *Nanotechnology*, 2014, **25**, 485706.

12 C. Pannu, U. B. Singh, S. Kumar, A. Tripathi, D. Kabiraj and D. K. Avasthi, *Appl. Surf. Sci.*, 2014, **308**, 193–198.

13 B. Pacakova, J. Vejpravova, A. Repko, A. Mantlikova and M. Kalbac, *Carbon*, 2015, **95**, 573-579.

14 C. Bautista-Flores, R. Y. Sato-Berrú and D. Mendoza, *Appl. Phys. Lett.*, 2014, **105**, 191116.

15 G. Jnawali, Y. Rao, J. H. Beck, N. Petrone, I. Kymissis, J. Hone and T. F. Heinz, *ACS Nano*, 2015, 150622103656000.

16 R. Wang, S. Wang, X. Wang, J. A. S. Meyer, P. Hedegard, B. W. Laursen, Z. Cheng and X. Qiu, *Small*, 2013, **9**, 2420–2426.

17 S. Morita, A. a Zakhidov and K. Yoshino, *Solid State Commun.*, 1992, **82**, 249–252.

18 J. Cho, J. Smerdon, L. Gao, O. Süzer, J. R. Guest and N. P. Guisinger, *Nano Lett.*, 2012, **12**, 3018–24.

19 C. Casiraghi, *Phys. Rev. B - Condens. Matter Mater. Phys.*, 2009, **80**, 2–4.

20 J. Vejpravova, B. Pacakova, J. Endres, A. Mantlikova, T. Verhagen, V. Vales, O. Frank and M. Kalbac, *Sci. Rep.*, 2015, 15161.

21 S. M. Choi, S. H. Jhi and Y. W. Son, *Phys. Rev. B*, 2010, **81**, 081407.

22 F. Guinea, M. I. Katsnelson and A. K. Geim, *Nat. Phys.*, 2009, **6**, 30–33.

23 M. A. Bissett, S. Konabe, S. Okada, M. Tsuji and H. Ago, *ACS Nano*, 2013, **7**, 10335–43.

24 A. K. Manna and S. K. Pati, *ChemPhysChem*, 2013, **14**, 1844–1852.

25 M. Kalbac, J. Kong and M. Dresselhaus, *J. Phys. Chem. C*, 2012, **116**, 19046.

26 O. Frank, L. Kavan and M. Kalbac, *Nanoscale*, 2014, **6**, 6363–70.

27 O. Frank, M. S. Dresselhaus and M. Kalbac, *Acc. Chem. Res.*, 2015, **48**, 111–118.

28 L. M. Malard, M. A. Pimenta, G. Dresselhaus and M. S. Dresselhaus, *Phys. Rep.*, 2009, **473**, 51–87.

29 J. E. Lee, G. Ahn, J. Shim, Y. S. Lee and S. Ryu, *Nat. Commun.*, 2012, **3**, 1024.

30 J. Zabel, R. R. Nair, A. Ott, T. Georgiou, A. K. Geim, K. S. Novoselov and C. Casiraghi, *Nano Lett.*, 2012, **12**, 617–21.

31 C. Galiotis, O. Frank, E. N. Koukaras and D. Sfyris, *Annu. Rev. Chem. Biomol. Eng.*, 2015, **6**, 121–140.

32 M. Lazzeri and F. Mauri, *Phys. Rev. Lett.*, 2006, **97**, 266407.

33 A. Das, S. Pisana, B. Chakraborty, S. Piscanec, S. K. Saha, U. V. Waghmare, K. S. Novoselov, H. R. Krishnamurthy, A. K. Geim, A. C. Ferrari and A. K. Sood, *Nat. Nanotechnol.*, 2008, **3**, 210–215.

34 J. Ek-Weis, S. Costa, O. Frank and M. Kalbac, *J. Phys. Chem. Lett.*, 2014, **5**, 549–554.

35 T. G. A. Verhagen, V. Vales, M. Kalbac and J. Vejpravova, *Phys. status solidi*, 2015, doi: 10.1002/pssb.201552223.

36 B. M. Ginzburg, M. V. Baidakova, O. F. Kireenko, D. G. Tochil'nikov and a. a. Shepelevskii, *Tech. Phys.*, 2000, **45**, 1595–1603.

37 A. Reina, X. Jia, J. Ho, D. Nezich, H. Son, V. Bulovic, M. S. Dresselhaus and J. Kong, *Nano Lett.*, 2009, **9**, 30–5.

38 M. Kalbac, O. Frank and L. Kavan, *Carbon N. Y.*, 2012, **50**, 3682–3687.

39 D. Nečas and P. Klapetek, *Cent. Eur. J. Phys.*, 2011, **10**, 181–188.

Figures and captions:

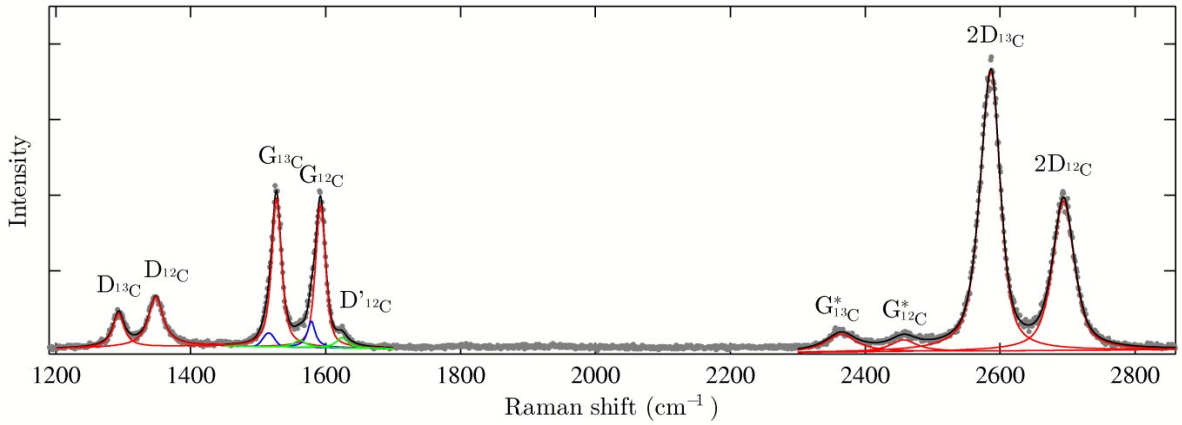

Fig. 1 A typical Raman spectrum of the ^{12}C graphene/C_{70}/^{13}C graphene heterostructure (grey dots). The red lines represent the fits of individual Raman bands of both isotopes. In the region around the G peaks, the D′ bands had to be fitted as well, as they overlap with the G peaks (green lines). The blue lines represent the G_2 peaks that were fitted because of the asymmetry of the main, G_1, peaks.

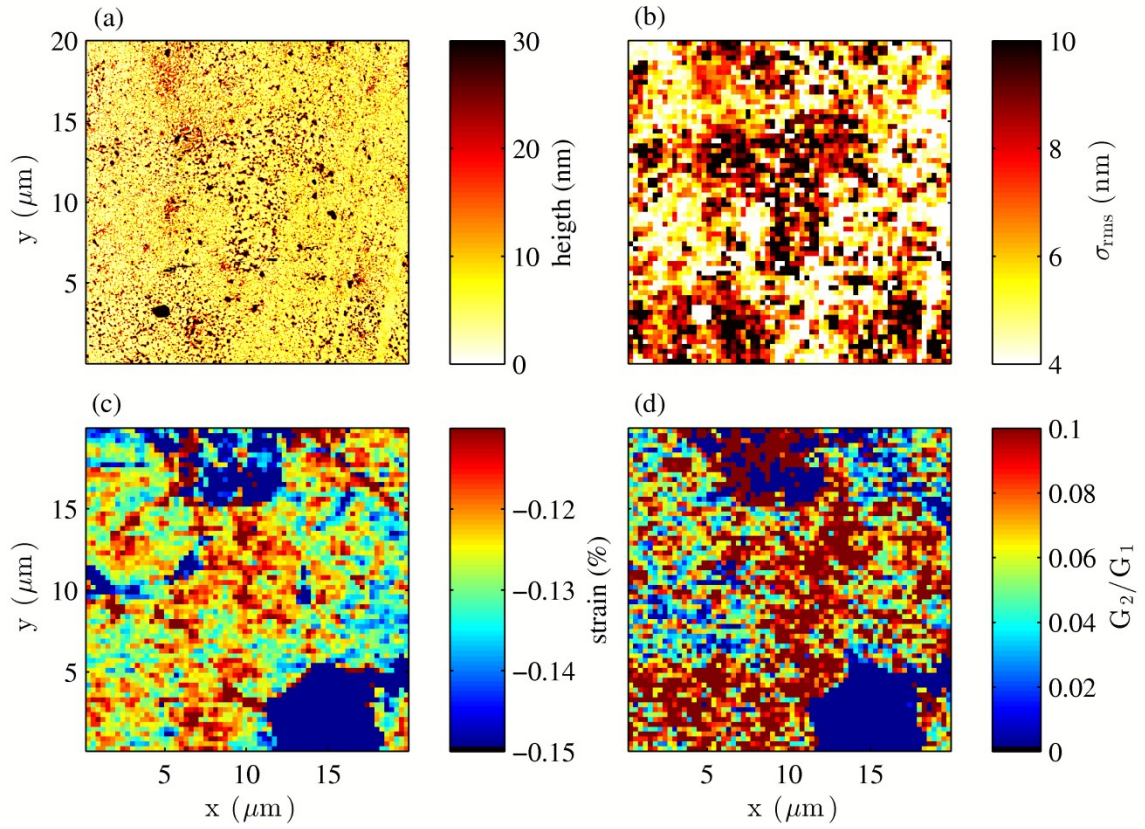

Fig. 2 The measured surface topography AFM map (a) and calculated local roughness from the AFM map spatially mapped onto the measured Raman data points (b). The map of strain in the ^{13}C top graphene layer calculated from the measured Raman data (c) and the map of the relative area of the G_2 peak of the ^{13}C top layer (d) .

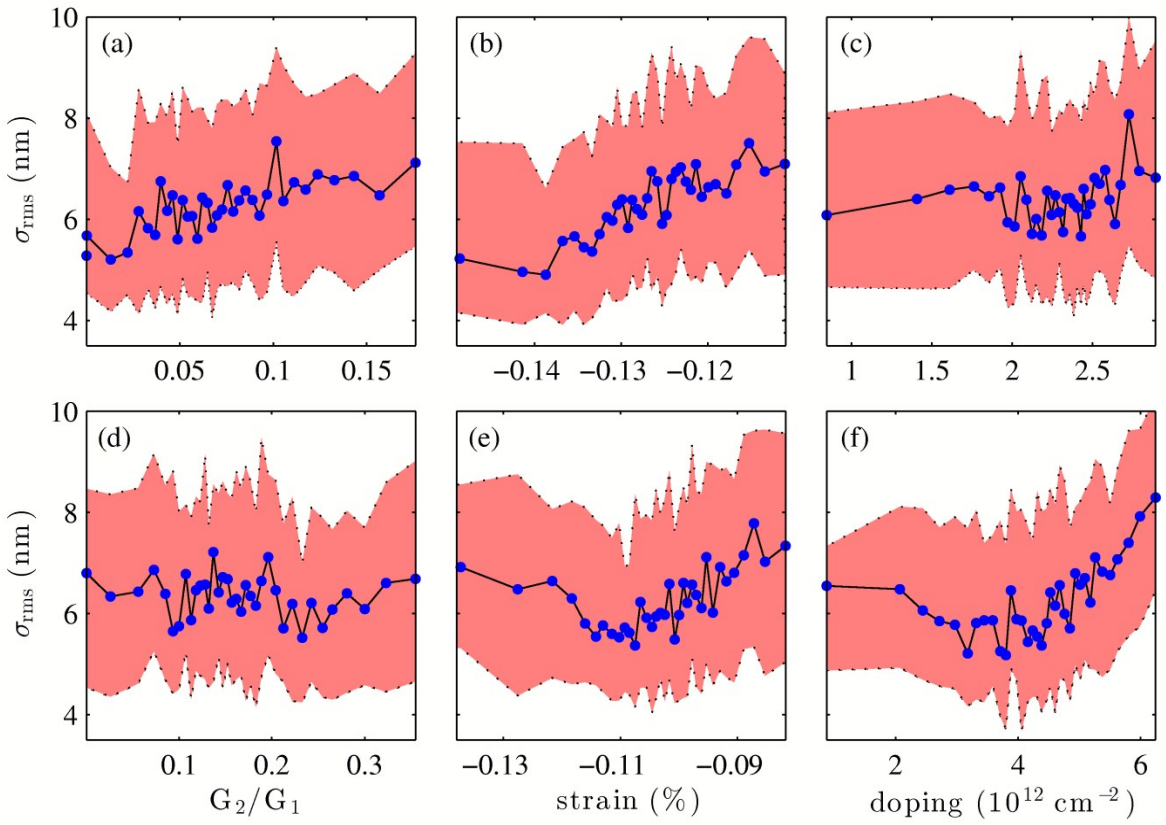

Fig. 3 A correlation plot of the local roughness (σ_{rms}) obtained by AFM and the parameters obtained from Raman mapping. Each adjacent 100 points of the correlation plot were binned together. The median (blue points) together with the first and third quartile (pink area) are depicted for the relative area of the G_2 peak (a), strain (b) and doping (c) of the ^{13}C top layer. For the bottom ^{12}C graphene layer, the relative area of the G_2 peak (d), strain (e) and doping (f) are shown as well.